arXiv:1301.5963v1 [cond-mat.str-el] 25 Jan 2013

Driven skyrmions and dynamical transitions in chiral magnets

Shi-Zeng Lin, Charles Reichhardt, Cristian D. Batista, and Avadh Saxena
Theoretical Division, Los Alamos National Laboratory, Los Alamos, New Mexico 87545, USA
(Dated: January 28, 2013)

We study the dynamics of skyrmions in chiral magnets in the presence of a spin polarized current. The motion of skyrmions in the ferromagnetic background excites spin waves and contributes to additional damping. At a large current, the spin wave spectrum becomes gapless and skyrmions are created dynamically from the ferromagnetic state, resulting in a liquid-like state of skyrmions. At an even higher current, these skyrmions are strongly deformed due to the damping and become unstable at a threshold current, leading to a paramagnetic-like state. We show how skyrmions can be created by increasing the current in the magnetic spiral state. We then construct a dynamic phase diagram for a chiral magnet with a spin polarized current. The instability transitions between different states can be observed as experimentally clear signatures in the transport measurements, such as jumps and hysteresis.

PACS numbers: 75.10.Hk, 75.25.-j, 75.30.Kz, 72.25.-b

Introduction – Skyrmions as topological objects were first proposed as a model for baryons [1] and were first realized experimentally in condensed matter systems in quantum-Hall ferromagnets. [2] Skyrmions were also predicted to be stable in chiral magnets, where the inversion symmetry is broken due to the spin-orbit coupling.[3–5] In this context, the spins wrap a sphere when one moves from the center of the skyrmion to infinity. Hexagonal skyrmion lattices were observed in the *A* phase of a metallic ferromagnet MnSi [6] as well as in compounds with a B20 structure [7, 8]. More recently skyrmion lattices have been directly imaged in thin films of $\mathrm{Fe_{0.5}Co_{0.5}Si}$ by Lorentz force microscopy [9], and these lattices were shown to be more stable than those in bulk materials. [10, 11] The continuing identification of more materials with skyrmion lattices suggests that they are ubiquitous in magnetic metals without inversion symmetry.

One of the main themes in the field of spintronics is the manipulation of spin texture by electric currents. The main player is magnetic domain walls (DWs) and their controlled motion by current is under active study. It has been shown [12] that the threshold current to move DWs is extremely high, on the order of $10^5 - 10^6$ A/cm^2, which is detrimental for applications due to the intensive Joule heating. Skyrmions are also promising candidates for the application of spintronics as information carriers, but their potential use for this purpose depends crucially on both controlled creation of skyrmions and manipulation of their motion. Skyrmions can be driven by a spin polarized current in a manner similar to DWs. Recently it was demonstrated experimentally that the threshold current to move a skyrmion is 4 to 5 orders of magnitude smaller than that required to move DWs [13–15], indicating that skyrmions could have a tremendous advantage over DWs since the Joule heating can be reduced significantly. Thus, an understanding of the dynamics of skyrmions is both necessary and timely, particularly the stability of the driven skyrmions and how fast they can be manipulated.

In this Letter, we study the motion of a single skyrmion in a ferromagnetic (FM) background and the flow of a skyrmion lattice in the presence of a spin polarized current. Due to the damping, the skyrmion acquires a velocity transverse to the current (skyrmion Hall effect). The motion of the skyrmion perturbs the FM background causing the radiation of a spin wave. This radiation is enhanced when the velocity of skyrmion reaches a threshold and the spin wave spectrum becomes gapless, leading to an instability where multiple skyrmions are created and the voltage, which is proportional to the number of skyrmions, increases sharply. At a higher current, the skyrmion structure is strongly distorted due to the damping and finally the skyrmions become unstable, resulting in a paramagnetic-like state with random and chaotic precession of spins. The ratio between the longitudinal and transverse voltages jumps at the instability. We also show that the skyrmion lattice can be dynamically created from the spiral state under current. Based on these results, a dynamic phase diagram for chiral magnets with spin polarized current is constructed. The onset of the different instability transitions can be observed from transport measurements in experiments, including pronounced jumps and hysteresis effects in the current-voltage curves.

Model – We consider a thin film of chiral magnets, which is described by the spin Hamlitonian with the Dzyaloshinskii-Moriya (DM) interaction in a dimensionless form [3–5, 16],

$$\mathcal{H} = \int d\mathbf{r}^2 \left[\frac{J_{\mathrm{ex}}}{2}(\nabla\mathbf{n})^2 + D\mathbf{n}\cdot\nabla\times\mathbf{n} - \mathbf{H}_a\cdot\mathbf{n}\right], \qquad (1)$$

where J_{ex} is the exchange constant, D is the DM interaction due to spin-orbit coupling [17–19], and the last term accounts for the Zeeman interaction with the external field $\mathbf{H}_a$. Here $\mathbf{n}(x, y)$ is a unit vector describing the direction of magnetic moment. The external field is perpendicular to the film $\mathbf{H}_a = H_a\hat{z}$. The phase diagram of chiral magnets obeying Eq. (1) at temperature $T = 0$ K is summarized as follows. [16] At $H_a = 0$, the system favors a spiral configuration of magnetic moments. Upon increasing H_a, the hexagonal skyrmion lattice is stabilized at $H_a > 0.2D^2/J_{\mathrm{ex}}$. At higher fields $H_a > 0.8D^2/J_{\mathrm{ex}}$, the ferromagnet becomes the ground state. Both transitions are of the first order.

In the presence of a spin polarized current, the localized moment experiences a spin transfer torque due to the conduction electrons. The dynamics of the magnetic moments is described by the Landau-Lifshitz-Gilbert equation [20–22]

$$\partial_t \mathbf{n} = (\mathbf{J}\cdot\nabla)\mathbf{n} - \gamma \mathbf{n}\times\mathbf{H}_{\mathrm{eff}} + \alpha\partial_t\mathbf{n}\times\mathbf{n}, \tag{2}$$

where the first term on the right hand side (r.h.s.) represents the spin-transfer torque with spin current density $\mathbf{J}$ and the last r.h.s. term is the Gilbert damping with damping coefficient α. [23] The effective field is $\mathbf{H}_{\mathrm{eff}} = -\delta\mathcal{H}/\delta\mathbf{n} = J_{\mathrm{ex}}\nabla^2\mathbf{n} - 2D\nabla\times\mathbf{n} + \mathbf{B}$. We solve [24] Eq. (2) numerically to obtain the current-voltage (I-V) characteristics with the electric field given by $\mathbf{E} = \mathbf{n}\cdot(\nabla\mathbf{n}\times\partial_t\mathbf{n})$. [25] The total number of skyrmions in the film is $Q = \int d\mathbf{r}^2 q(\mathbf{r})$ with the skyrmion density $q = \mathbf{n}\cdot(\partial_x\mathbf{n}\times\partial_y\mathbf{n})/(4\pi)$. [26]

Dynamics of a single skyrmion – Let us first consider the motion of a single skyrmion. In the absence of damping $\alpha = 0$, Eq. (2) has an exact solution $\mathbf{n}_S(\mathbf{r}-\mathbf{v}t)$ with $\mathbf{v} = -\mathbf{J}$, where $\mathbf{n}_S(\mathbf{r})$ is the structure of the skyrmion in the static case $J = 0$. This solution corresponds to the comoving of skyrmion and conduction electrons, therefore the spin-transfer torque is zero. Thus without damping, the structure of a moving skyrmion is the same as that at rest and its velocity is equal to $-\mathbf{J}$. With damping $\alpha > 0$, the structure of the skyrmion deforms. For low velocities, however, we can use the quasi-static approximation that the structure of the skyrmion is the same as that in the static case. The velocity of the skyrmion is given by [25]

$$\mathbf{v} = -\mathbf{J} - \alpha\eta\hat{\mathbf{z}}\times\mathbf{v} \tag{3}$$

with $\eta = \eta_\mu = 4\pi[\int d\mathbf{r}^2(\partial_\mu\mathbf{n})^2]^{-1}$ and $\mu = x,\ y$. The skyrmion acquires a velocity component perpendicular to the current due to the damping. The velocity parallel to the current is $v_\parallel = -J/(1+\alpha^2\eta^2)$ and the perpendicular velocity is $v_\perp = J\alpha\eta/(1+\alpha^2\eta^2)$. The corresponding voltages across the skyrmion are $V_\parallel = -4\pi v_y$ and $V_\perp = 4\pi v_x$. Thus the viscosity of the skyrmion is $\eta_v \equiv J/v = \sqrt{1+\alpha^2\eta^2}$, and the Hall angle is $\theta_H \equiv \tan^{-1}(v_\perp/v_\parallel) = -\tan^{-1}(\alpha\eta)$. We calculate the Hall angle and velocity numerically to check Eq. (3). The velocity is defined as $\mathbf{v} = \dot{\mathbf{s}}(t)$ with $\mathbf{s}$ the center of mass $\mathbf{s} = \frac{1}{Q}\int d\mathbf{r}^2 q(\mathbf{r})\mathbf{r}$. We initialize a skyrmion in the FM background in the film and then ramp up the current gradually. At a small current (velocity), the numerical results of Hall angle and velocity are consistent with the analytical calculations, as shown in Fig. 1. The motion of the skyrmion is different from that of a superconducting vortex, where the velocity is perpendicular to the current. [27]

When the current (velocity) increases, the skyrmion starts to deform, especially when α is large, and thus the quasi-static approximation in Eq. (3) becomes questionable. We calculate numerically the I-V curve with a single skyrmion at $J = 0$ as an initial state. The resulting I-V curve and dependence of Q on J are shown in Fig. 2 (a-c). For a small current, the motion of the skyrmion is stable, as shown in Fig. 2(d). The movement of the skyrmion perturbs the ferromagnetic background and excites spin wave excitations. The effect of the radiation of a spin wave is more prominent when the skyrmion is accelerated or decelerated by a time-dependent current or scattered by impurities. Let us consider the motion of a skyrmion in the FM background, which radiates a spin wave $\mathbf{n} = \hat{z} + \delta$ with $\delta \ll 1$. The dynamics of δ is

$$i(\omega - \mathbf{J}\cdot\mathbf{k})\delta_x = -\gamma\left(H_a + J_{\mathrm{ex}}\mathbf{k}^2 + i\alpha\omega/\gamma\right)\delta_y + h_{S,x}(\omega,\mathbf{k}), \tag{4}$$

$$i(\omega - \mathbf{J}\cdot\mathbf{k})\delta_y = \gamma\left(H_a + J_{\mathrm{ex}}\mathbf{k}^2 + i\alpha\omega/\gamma\right)\delta_x + h_{S,y}(\omega,\mathbf{k}), \tag{5}$$

where $h_{S,\mu}(\omega,\mathbf{k}) = h_{S,\mu}(\omega,\mathbf{k})\delta(\omega - \mathbf{v}\cdot\mathbf{k})$ is the effective field induced by the motion of the skyrmion. Maximal radiation occurs when the resonance condition $\Omega(\mathbf{k}) = \mathbf{v}\cdot\mathbf{k}$ is satisfied, where

$$\Omega(\mathbf{k}) = \mathbf{J}\cdot\mathbf{k} \pm \frac{J_{\mathrm{ex}}\gamma\mathbf{k}^2 + \gamma H_a}{1+\alpha^2}, \tag{6}$$

is the spin wave spectrum determined from Eqs. (4) and (5) with $h_{S,\mu}(\omega,\mathbf{k}) = 0$. It requires a threshold current J_r above which the resonance condition $\Omega(\mathbf{k}) = \mathbf{v}\cdot\mathbf{k}$ can be satisfied. For weak damping $\alpha \ll 1$ where $\mathbf{v} \approx -\mathbf{J}$, $J_r = \gamma\sqrt{H_a J_{\mathrm{ex}}}/(\alpha^2+1)$. The dominant wave vector is $k_x = \sqrt{H_a/J_{\mathrm{ex}}}$ and $k_y = 0$. One typical configuration of n_x is illustrated in Fig. 3 which clearly shows the radiation of the spin wave due to the motion of the skyrmion. For strong damping, the excited spin wave decays quickly because the amplitude of the spin wave decreases with the damping constant α. The radiation of spin waves thus gives an additional contribution to the damping of skyrmion. According to the simulations, this contribution is small because the amplitude of the spin wave is weak. The radiation of collective excitations due to the motion of driven topological objects is well known in other systems, such as Josephson junctions [28] and DWs [29, 30].

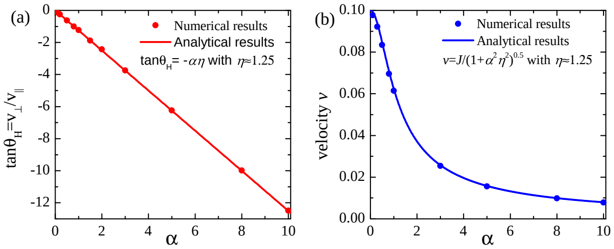

FIG. 1. (color online) (a) The Hall angle $\tan\theta_H$ and (b) the velocity v vs α for the motion of a single skyrmion obtained numerically (dots) and analytically (lines) at $J = 0.1$.

The spin wave excitation spectrum $\Omega(\mathbf{k})$ [Eq. (6)] becomes gapless when the applied current reaches the value $J_m = 2\gamma\sqrt{H_a J_{\mathrm{ex}}}/(\alpha^2+1)$. This gapless condition signals an instability of the FM state into a helical state whose xy-spin component has spiral correlations with wave vector $\boldsymbol{k}_m = (k_x = \sqrt{H_a/J_{\mathrm{ex}}}, k_y = 0)$. Simulations show that the amplitude of the spiral xy-component grows until the partially saturated FM state is destroyed via proliferation of multiple

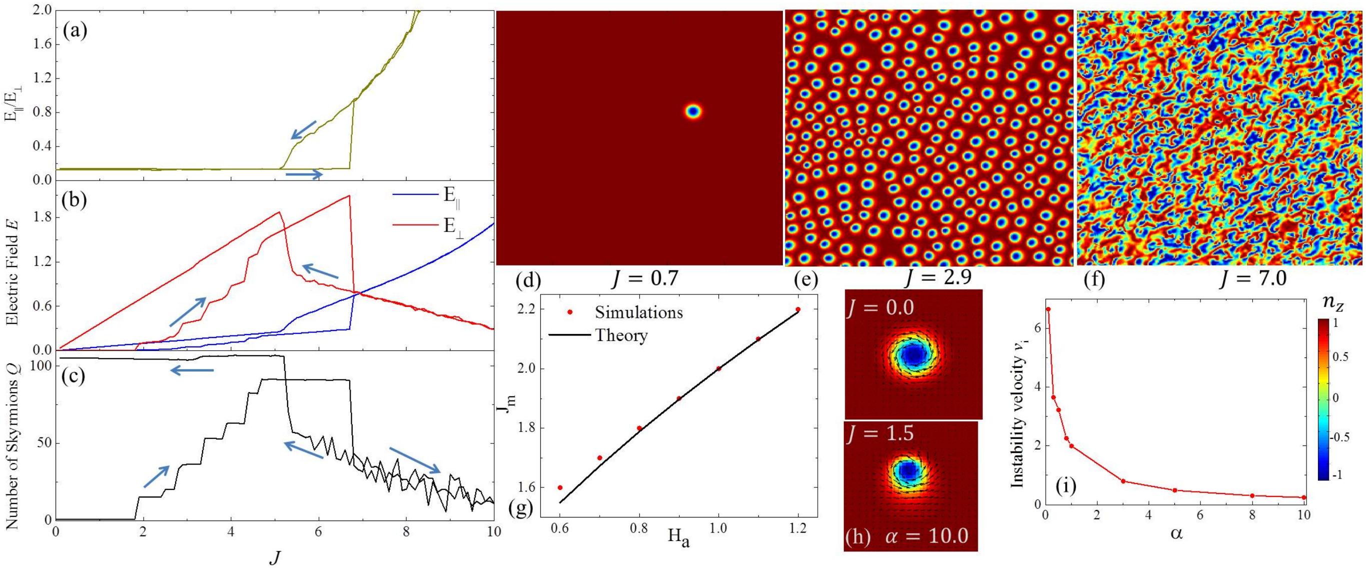

FIG. 2. (color online) (a) $E_\parallel/E_\perp$, (b) electric field E, and (c) total number of skyrmions Q vs the spin current J. The arrows indicate the direction of current sweep. (d-f) Configurations of n_z in the case of (d) a single skyrmion, (e) multiple skyrmions, and (f) the paramagnetic phase at different currents. Here $\alpha = 0.1$. (g) Comparison between analytical (line) and numerical (dots) results for the current J_m at which the instability occurs and multiple skyrmions are created. (h) Comparison between spatial structure of a skyrmion at rest and at a large current, showing distortion. The vectors in the plots denote the n_x and n_y components, and color denotes the n_z component. (i) The velocity v_i where skyrmions become unstable vs α.

skyrmions [see Figs. 2 (c) and 2 (e)]. The presence of a moving skyrmion affects the relaxation of the original FM state into the skyrmion-rich state in the neighborhood of the moving skyrmion because spin fluctuations are locally enhanced via radiation of spin waves. The amplitude of the $\boldsymbol{k} = \boldsymbol{k}_m$ spin wave keeps increasing until more skyrmions are created around the original moving skyrmion. The new skyrmions move in response to the applied current and radiate spin waves that create a new generation of skyrmions. This multiplicative process repeats, until the system is filled with a finite concentration of skyrmions. The electric field increases in a series of steps [Fig. 2 (b)] because it is proportional to the number of skyrmions Q that increases in the same way [see Fig. 2 (c)]. The change of current does not modify the direction of motion because the ratio $E_\parallel/E_\perp$ is independent of J [Fig. 2 (a)]. Figure 2 (g) shows that our analytical expression for J_m reproduces the current value that is obtained from our simulations (i.e. value required to trigger the proliferation of multiple skyrmions).

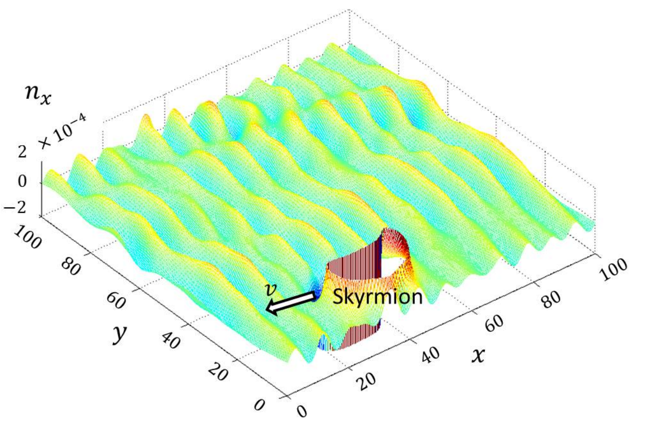

FIG. 3. (color online) Spatial structure of the n_x component of the spin wave radiated due to the motion of a skyrmion. The skyrmion location is labeled and the arrow denotes the direction of skyrmion motion. Here $\alpha = 0.1$, $J = 1.4$ and $H_a = 0.6$.

The skyrmion is no longer a circular object under large current and develops a tail opposite to the direction of motion, as shown in Fig. 2 (h). The distortion is stronger for larger α. At an even higher current, the structure of the skyrmion is so strongly distorted that the skyrmion becomes unstable. Here the relation $E_\perp/E_\parallel = -\alpha\eta$ breaks down as shown in Fig. 2 (a), indicating that there is an upper velocity limit for skyrmion motion due to the distortion induced by damping. Above this limit, the resulting state has random and chaotic precession of the magnetic moments and the configuration looks like a paramagnetic phase [Fig. 2 (f)]. When the current is reduced, the system recovers to a skyrmion phase at a current smaller than that at which the skyrmion was lost in the ramping up process, indicating the occurrence of hysteresis. As the current is further reduced, the number of skyrmions remains constant down to $J = 0$. The velocity v_i where the skyrmions become unstable decreases with the damping constant α as $v_i \sim 1/\sqrt{1 + \alpha^2\eta^2}$, as shown in Fig. 2(i). The distortion mediated instability of a topological object has been demonstrated in other systems, such as Larkin-Ovchinnikov instability of the vortex lattice in superconductors [31] and Walker break-

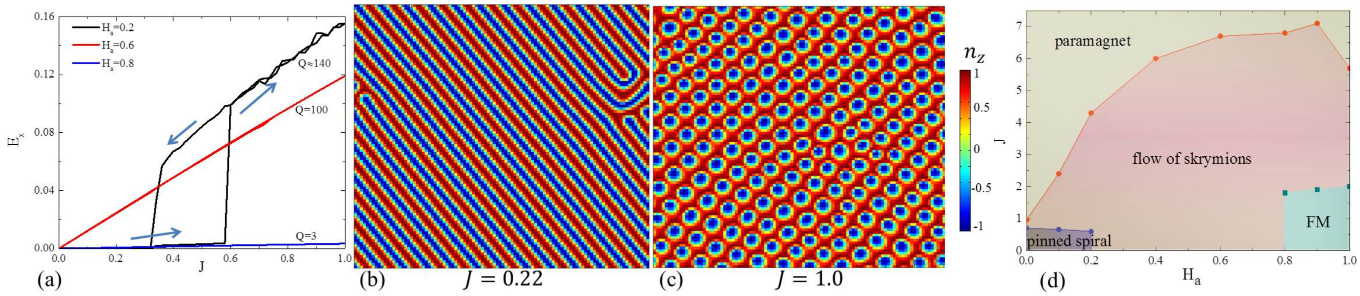

(a) (b) $J = 0.22$ (c) $J = 1.0$ (d)

FIG. 4. (color online) (a) Dependence of the longitudinal electric field E_x on spin current at different fields $H_a = 0.2$, $H_a = 0.6$, and $H_a = 0.8$. For $H_a = 0.2$, the number of skyrmions Q is not conserved at high currents and only an averaged value of Q is given. Arrows denote the direction of current sweep. (b-c) Configurations n_z for (b) the spiral phase and (c) the skyrmion lattice obtained with $H_a = 0.2$. The spiral phase is not perfect and contains some defects (right part of the plot) after the annealing process. (d) Dynamic phase diagram for J vs H_a of a chiral magnet obeying the Hamiltonian in Eq. (1) in the presence of a spin current. Here $\alpha = 0.1$.

down of DWs [32].

Dynamics Starting from the Ground State Configurations– In order to understand how the creation and destruction of the current driven states could be observed experimentally, we next consider the dynamics starting from the ground state configurations. The ground states are prepared carefully by numerical annealing from high temperature to zero temperature, where we find a low field magnetic spiral phase, an intermediate field skyrmion lattice, and a high field uniform ferromagnetic phase. In the ferromagnetic phase, the effect of the current vanishes since $\nabla \cdot \mathbf{n} = 0$ in this case, so that $\mathbf{E} = 0$. With fluctuations, the current couples with the fluctuations of magnetization and creates skyrmions at J_m where the spectrum of spin waves becomes gapless. The I-V curves for the spiral and skyrmion phases are shown in Fig. 4(a). For a small current, the spiral structure does not move and no voltage is induced in the system, as illustrated in Fig. 4 (b). This intrinsic pinning of the spiral structure is due to the DM interaction. Let us consider a spiral structure along the x direction $\mathbf{n} = (0,\ \cos(qx),\ \sin(qx))$, where q is the wave number of the spiral structure. The spin-transfer torque is $J_x q(0,\ -\sin(qx),\ \cos(qx)) = -\gamma \mathbf{n} \times \mathbf{H}_s$ with $\mathbf{H}_s = J_x q \hat{x}/\gamma$. Thus the effect of the spin transfer torque is equivalent to a magnetic field along the x direction. This field tends to align the spins along the x direction due to the Gilbert damping term, which costs energy as a result of the DM interaction. Thus, intrinsic pinning of skyrmions exists in clean systems [33], similar to the case of DWs [34].

As the current is increased, the spiral structure becomes unstable and a lattice of skyrmions emerges above a critical current, as shown in Fig. 4 (c). At $J \approx 0.34$, a small number of skyrmions ($Q = 5$) is created while most of the system retains the spiral structure. At $J \approx 0.6$, the remaining spiral structure is converted into the skyrmion lattice. These skyrmions move freely under an applied current, which induces transverse and longitudinal electric fields. The electric fields are proportional to the number of skyrmions, so they decrease with increasing H_a because the skyrmion density decreases. When the current is increased further, the skyrmion becomes unstable and the system evolves into the paramagnetic phase discussed above. At low fields where the spiral structure is the ground state, hysteresis occurs upon decreasing the current, while at high fields where the skyrmion lattice is the ground state, no hysteresis is observed. From these results, we construct a dynamic phase diagram for chiral magnets in a magnetic field under spin polarized current, as shown in Fig. 4 (d). There is hysteresis when the current is swept across the phase boundary, so we show the location of the boundary obtained for increasing current. The hysteresis indicates that the transition between different phases has first order features.

Discussion – Using typical parameters, we estimate the current density at which the instabilities of skyrmion destruction occur. The current in Eq. (2) is given in units of $\gamma e M_s^2 \xi/\mu_B$, where $M_s \approx 10^3$ Gauss is the saturation magnetization, $\gamma \approx 10^7$ Gauss^{-1}s^{-1} is the gyromagnetic ratio [21], $\xi \approx 10$ nm is the size of the skyrmion [9], e is the elementary charge, and μ_B is the Bohr magneton. We thus estimate the instability occurs at a current of order 10^8 A/m^2, which is easily experimentally accessible. The fastest possible velocity for skyrmions is of the order of $\xi\gamma M_s \sim 100$ m/s for a weak damping $\alpha \ll 1$ and it decreases as $1/\sqrt{1+\alpha^2\eta^2}$. The Joule heating could be minimized by using a pulse current. To examine the instability and motion of a single skyrmion in the FM background it should be possible to create a single skyrmion experimentally by applying a local magnetic field or a circular current [35].

We emphasize that the dynamic phase transition at $J = J_m$ occurs regardless of the existence of a skyrmion in the original ($J = 0$) FM state. The creation of skyrmions at J_m can also be induced by other relaxation mechanisms, such as spin fluctuations induced by coupling to the lattice and conduction electrons. Such fluctuations provide the dominant relaxation mechanism far away from the moving skyrmion. The dynamical creation of skyrmions by current happens even at strong magnetic fields where the ground state is FM at $J = 0$, which points to a possibly robust way to create skyrmions experimentally. In experiments, this dynamical transition can be observed by transport measurements or neutron scattering. Moreover, the resulting skyrmions form a liquid-like state, which has not yet been realized experimentally by only applying external magnetic fields. This new skyrmion liquid state opens a door for the investigation of skyrmions in the disordered state.

We thank Yasuyuki Kato, Leonardo Civale for useful discussions and Cynthia Reichhardt for a critical reading of the manuscript. This work was carried out under the auspices of the NNSA of the US DoE at LANL under Contract No. DE-AC52-06NA25396, and was supported by the US Department of Energy, Office of Basic Energy Sciences, Division of Materials Sciences and Engineering.

[1] T. H. R. Skyrme, Proc. R. Soc. London, Ser. A **260**, 127 (1961).
[2] S. E. Barrett, G. Dabbagh, L. N. Pfeiffer, K. W. West, and R. Tycko, Phys. Rev. Lett. **74**, 5112 (1995).
[3] A. N. Bogdanov and D. A. Yablonskii, Sov. Phys. JETP **68**, 101 (1989).
[4] A. Bogdanov and A. Hubert, J. Magn. Magn. Mater. **138**, 255 (1994).
[5] U. K. Röß ler, A. N. Bogdanov, and C. Pfleiderer, Nature **442**, 797 (2006).
[6] S. Mühlbauer, B. Binz, F. Jonietz, C. Pfleiderer, A. Rosch, A. Neubauer, R. Georgii, and P. Böni, Science **323**, 915 (2009).
[7] W. Münzer, A. Neubauer, T. Adams, S. Mühlbauer, C. Franz, F. Jonietz, R. Georgii, P. Böni, B. Pedersen, M. Schmidt, A. Rosch, and C. Pfleiderer, Phys. Rev. B **81**, 041203 (2010).
[8] C. Pfleiderer, T. Adams, A. Bauer, W. Biberacher, B. Binz, F. Birkelbach, P. Böni, C. Franz, R. Georgii, M. Janoschek, F. Jonietz, T. Keller, R. Ritz, S. Mühlbauer, W. Münzer, A. Neubauer, B. Pedersen, and A. Rosch, J. Phys.: Condens. Matter **22**, 164207 (2010).
[9] X. Z. Yu, Y. Onose, N. Kanazawa, J. H. Park, J. H. Han, Y. Matsui, N. Nagaosa, and Y. Tokura, Nature **465**, 901 (2010).
[10] S. D. Yi, S. Onoda, N. Nagaosa, and J. H. Han, Phys. Rev. B **80**, 054416 (2009).
[11] X. Z. Yu, N. Kanazawa, Y. Onose, K. Kimoto, W. Z. Zhang, S. Ishiwata, Y. Matsui, and Y. Tokura, Nature Materials **10**, 106 (2011).
[12] M. Yamanouchi, D. Chiba, F. Matsukura, and H. Ohno, Nature **428**, 539 (2004).
[13] F. Jonietz, S. Mühlbauer, C. Pfleiderer, A. Neubauer, W. Münzer, A. Bauer, T. Adams, R. Georgii, P. Böni, R. A. Duine, K. Everschor, M. Garst, and A. Rosch, Science **330**, 1648 (2010).
[14] X. Z. Yu, N. Kanazawa, W. Z. Zhang, T. Nagai, T. Hara, K. Kimoto, Y. Matsui, Y. Onose, and Y. Tokura, Nature Communications **3**, 988 (2012).
[15] T. Schulz, R. Ritz, A. Bauer, M. Halder, M. Wagner, C. Franz, C. Pfleiderer, K. Everschor, M. Garst, and A. Rosch, Nature Physics **8**, 301 (2012).
[16] J. H. Han, J. Zang, Z. Yang, J.-H. Park, and N. Nagaosa, Phys. Rev. B **82**, 094429 (2010).
[17] I. Dzyaloshinsky, J. Phys. Chem. Solids **4**, 241 (1958).
[18] T. Moriya, Phys. Rev. **120**, 91 (1960).
[19] T. Moriya, Phys. Rev. Lett. **4**, 228 (1960).
[20] Y. B. Bazaliy, B. A. Jones, and S.-C. Zhang, Phys. Rev. B **57**, R3213 (1998).
[21] Z. Li and S. Zhang, Phys. Rev. Lett. **92**, 207203 (2004).
[22] G. Tatara, H. Kohno, and J. Shibata, Phys. Rep. **468**, 213 (2008).
[23] There is additional damping due to the electric fields induced by the motion of skyrmions [25], which can be taken into account by using an effective damping coefficient.
[24] In simulations, we take $J_{\text{ex}} = D = \gamma = 1$. The size of the simulation box is $L \times L = 100 \times 100$. The system is discretized with grid size 0.4; a smaller grid size is also used to check the accuracy of the results. We use periodic boundary condition in both directions. To find the ground state, we anneal the system by adding a Gaussian noise field along the z direction in $\mathbf{H}_{\text{eff}}$. Equation (2) is solved by an explicit numerical scheme developed in Ref. 36. The spin current is along the x direction.
[25] J. Zang, M. Mostovoy, J. H. Han, and N. Nagaosa, Phys. Rev. Lett. **107**, 136804 (2011).
[26] A. Alexander and B. D. Simons, *Condensed Matter Field Theory* (Cambridge University Press, Cambridge, 2010).
[27] M. Tinkham, *Introduction to Superconductivity* (McGraw-Hill, Inc., New York, 1996).
[28] X. Hu and S. Z. Lin, Supercond. Sci. Technol. **23**, 053001 (2010).
[29] D. Bouzidi and H. Suhl, Phys. Rev. Lett. **65**, 2587 (1990).
[30] R. Wieser, E. Y. Vedmedenko, and R. Wiesendanger, Phys. Rev. B **81**, 024405 (2010).
[31] A. I. Larkin and Y. N. Ovchinnikov, Soviet Physics JETP **20**, 762 (1965).
[32] N. L. Schryer and L. R. Walker, J. Appl. Phys. **45**, 5406 (1974).
[33] J. Iwasaki, M. Mochizuki, and N. Nagaosa, arXiv:1207.3224 (2012).
[34] G. Tatara and H. Kohno, Phys. Rev. Lett. **92**, 086601 (2004).
[35] Y. Tchoe and J. H. Han, Phys. Rev. B **85**, 174416 (2012).
[36] C. Serpico, I. D. Mayergoyz, and G. Bertotti, J. Appl. Phys. **89**, 6991 (2001).